Journal Name

ARTICLE

Hydrazone-modulated peptides for efficient gene transfection

Iria Louzao,[a] Rebeca García-Fandiño[a,b] and Javier Montenegro*[a]

Received 00th January 20xx,
Accepted 00th January 20xx

DOI: 10.1039/x0xx00000x

www.rsc.org/

Gene transfection continues to be a major challenge in chemistry, biology and materials sciences. New methodologies and recent breakthroughs have renewed the interest in the discovery and development of new tools for efficient gene transfection. The hydrazone formation between a cationic head and hydrophobic tails has emerged as one of the most promising techniques for nucleotide delivery. In this contribution, we have exploited hydrazone formation to modulate the transfection activity of a parent linear peptide in combination with a plasmid DNA cargo. This strategy allowed the straightforward preparation, in physiological compatible conditions, of a discrete library of amphiphilic modulated penetrating peptides. Without the requirement of any isolation or purification steps, these modulated amphiphilic peptides were combined with a plasmid DNA and screened in transfection experiments of human HeLa cells. Three of these hydrazone-conjugated peptides were identified as excellent vectors for plasmid delivery, with comparable, or even higher efficiencies, and lower toxicity than the commercial reagents employed in routine transfection assays.

Introduction

The combined efforts of biology, chemistry and materials sciences have permitted the manipulation of the genetic machinery of the cell.[1-5] Although substantial advances have been made, we are still far from realizing the great potential that genetic manipulation will have for the future of humankind. Continuous breakthroughs and the development of different technologies have permanently been fuelling the field of genetic engineering and gene therapy.[1,4,5] Currently, the tool set for genetic manipulation can be divided into two main groups: transient active molecules and genome edition. The first group employs transient molecules such as poly or oligo-nucleotides to modulate gene expression.[1] The second group of editing techniques comprises several programmable nucleases such as the zinc fingers, the transcription activator–like effectors (TALENs) and the CRISPR-associated nuclease Cas9.[2]

The application of transient active nucleotides for genetic modifications started with the introduction (*transfection*) of exogenous recombinant plasmid DNAs inside cells.[4] In these protocols, the foreign DNA is delivered inside the nucleus to access the transcription machinery of the cell for the subsequent mRNA synthesis and protein expression. The following antisense techniques were based in the delivery of a single stranded oligonucleotide that binds the messenger RNA (mRNA), which is therefore inhibited for protein translation.

The discovery of the RNA interference mechanism (RNAi) has triggered new opportunities for genetic manipulation by interfering the gene expression at the cytoplasm post-transcriptional level.[1,3,6] Among these techniques we can find small interfering RNA (siRNA) and microRNAs. In general, the siRNA is a short exogenous double stranded oligonucleotide of about 20-25 base pairs. After delivery in the cytoplasm, the siRNA is processed by an enzyme called DICER and then integrated into the RNA-induced silencing complex (RISC). The RISC complex chops the target mRNA in small pieces, a process that finally results in the inhibition of the synthesis of the corresponding encoded protein.[6] On the other hand, microRNAs are single stranded oligonucleotides that are endogenously produced and processed by the cell in order to bind, sometimes promiscuously, to one or more mRNAs and inhibit the corresponding protein synthesis.[7] Recently, the delivery of mRNAs has also emerged as a promising technique for the transient expression of the therapeutic protein of interest.[8] This methodology avoids permanent recombination and allows the control over the protein expression until the mRNA is degraded.

Finally, the rising genome-editing techniques require the expression (or delivery) of nucleases, which are enzymes that catalyse DNA cleavage.[2] Most commonly, these nucleases are designed to specifically recognise a particular loci in the genome and generate double strand breaks that can be edited by different cellular repair mechanisms. The simplicity and specificity of the CRISPR approach turn this technique as the most promising strategy towards gene

[a] *Singular Research Centre in Chemical Biology and Molecular Materials (CIQUS), Organic Chemistry Department, University of Santiago de Compostela (USC), Santiago de Compostela, Spain.*

[b] *Centro de de Investigação em Química da Universidade do Porto (CIQUP), Department of Chemistry and Biochemistry, Faculty of Sciences, University of Porto, R. Campo Alegre, s/n, P-4169-007 Porto, Portugal.*

** Correspondence should be addressed to: javier.montenegro@usc.es*

Electronic Supplementary Information (ESI) available: [details of any supplementary information available should be included here]. See DOI: 10.1039/x0xx00000x

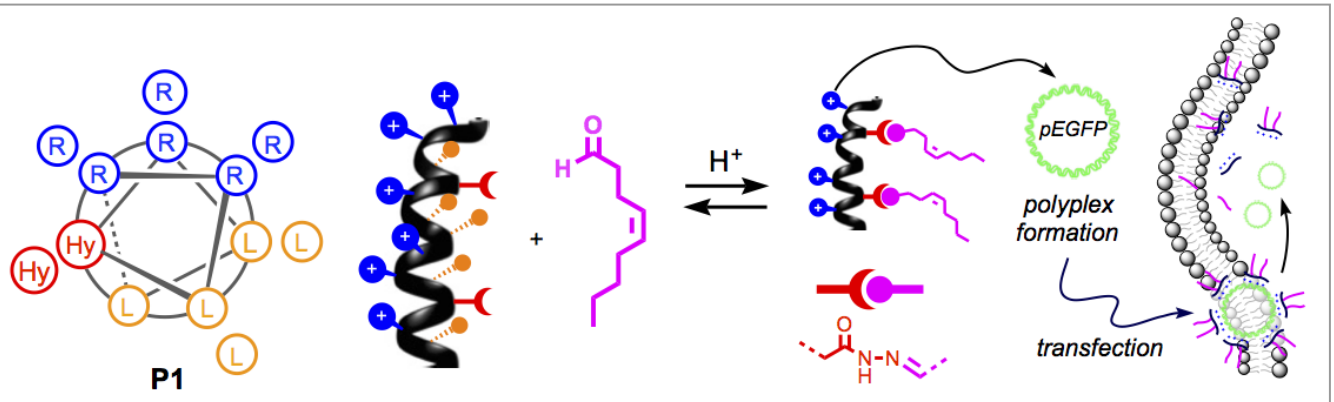

Figure 1. Heptad-based wheel diagram for the potential helical conformation of peptide **P1**. Representation of the potential amphiphilic helical structure bearing two reactive hydrazides (in red). Treatment of **P1** with a hydrophobic aldehyde affords an amphiphilic cationic peptide that complexes, transports and delivers a plasmid DNA across the membrane of HeLa cells. Colour code: Arginine: blue; leucine: orange; hydrazide: red; hydrophobic aldehyde: purple; pEGFP-C1 plasmid DNA: green.

edition.[2] Paradoxically, the most efficient CRISPR genome edition is achieved by the transfection of the plasmids that encode for the corresponding nucleases.[2] It is therefore of critical importance to innovate and to expand the chemical tool set for plasmid and polynucleotide intracellular delivery.

However, despite all the advances that have already been achieved, the previously described techniques suffer from important limitations. These could be related to the nucleotide cargo or to the delivery vehicle.[1,4,5,9] The nucleotide cargo suffers from either potential permanent recombination of plasmids, from the sensitivity towards nuclease degradation of short oligonucleotides such as siRNA and from the problematic immunological response that can be triggered for any kind of nucleotide.[5] The delivery vehicle can be either a viral or a non-viral vector.[1,3,5,10] Although efficient and in some cases also selective, viral vectors have important limitations related to their potential biosafety concerns, their immunogenicity and the low levels of the DNA packaging capacity.[3-5] As an alternative, different non viral vectors have been developed to achieve and improve nucleotide delivery,[1,3,11] which include lipids,[12-14] peptides,[15-24] nanoparticles,[12,25] polymers[26-29] and supramolecular systems.[30-33] However, non-viral vectors still present important barriers to overcome such as the poor packing and protection of the nucleotide cargo, the low stability of the resulting complex, the immune response, the escape from the endocytic route and most importantly, the low efficiency and the high cytotoxicity.[1,3]

Since the discovery of cell penetrating peptides, these cationic, sometimes amphiphilic, oligomers have shown a great potential for the delivery of different nucleotide cargos in cells and tissues.[9,16,18,24,34-36] The field of nucleotide intracellular delivery by penetrating peptides has been developed by important contributions of authors such as Szoka, Divita, Deshayes, Andaloussi, Futaki, Langel, Gait, Dowdy and many others.[9,16,18,24,36] The peptide vector can be covalently attached or non-covalently conjugated to the nucleotide cargo. In the later case, the nanoparticles formed, the polyplexes, exploit the ion pairing that is established between the anionic cargo and the cationic peptide.[16] As with the DNA/lipid formulations (lipoplexes) the peptides that form efficient polyplexes generally require the presence of hydrophobic residues that lead to the formation of amphiphilic nanoparticles.[16]

The hydrazone linkage between a polar head and one (or more) hydrophobic tails constitute one of the most promising approaches for the rapid synthesis and screening of amphiphilic nucleotide membrane transporters.[27,28,37-40] This strategy has already been employed for the delivery of siRNA by peptide dendrons[28] and polymers.[27] However, the hydrazone linkage has not been so far applied to the modulation of linear peptide sequences. Furthermore, although this methodology afforded efficient transfecting reagents for small double stranded nucleotides (i.e. siRNA), the same molecules that delivered short RNAs failed for the transfection of high molecular weight DNA plasmids in living cells.[27,28]

In this paper, we exploit the concept of hydrazone activation for the transfection, for the first time, of a plasmid DNA by a cationic linear peptide template (Fig. 1). This parent peptide, bearing hydrazyde connectors, was combined with a broad range of aldehyde tails for the straightforward preparation and screening of hydrazone-modulated peptides for the delivery of plasmid DNA in living cells. We demonstrate the suitability of this methodology for the identification of excellent peptide vehicles that work with similar or even higher efficacy and lower toxicity than the routine commercial reagents (e.g. Lipofectamine 2000).

Results

Design and peptide synthesis. The peptide scaffold was prepared by solid phase peptide synthesis using a standard Fmoc solid phase strategy (Fig. 2 and ESI).[41] Briefly, we started from a Rink amide solid support, which was subjected to consecutive deprotection and coupling cycles for the growth of the linear peptide sequence that was terminated by acetylation of the N-terminus (Fig. 2). The

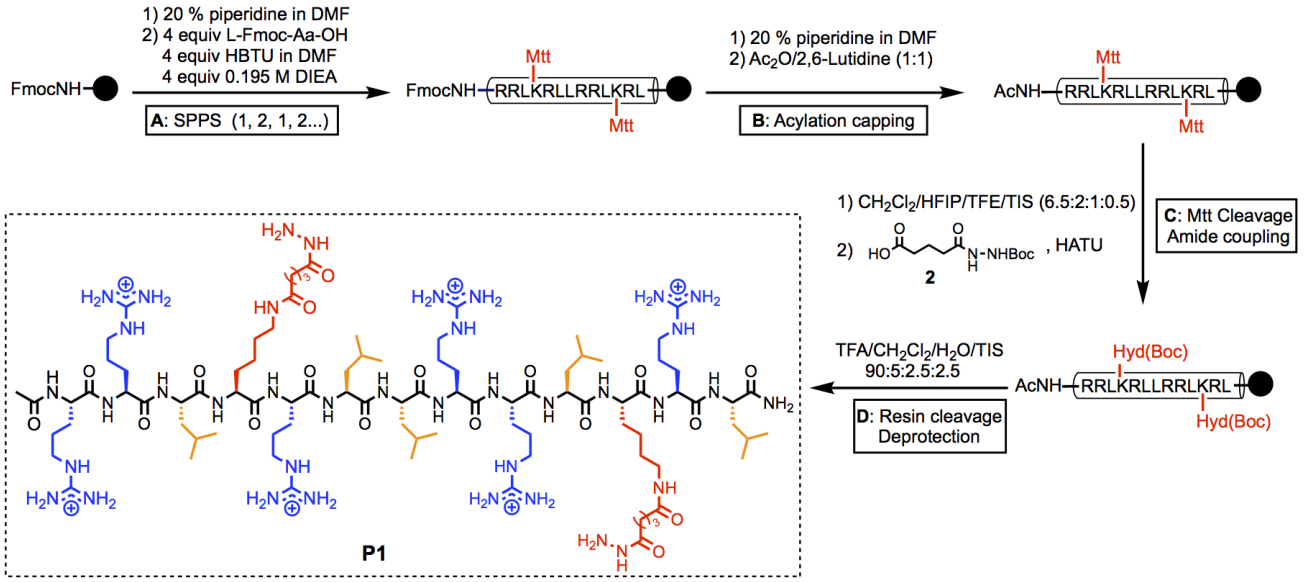

Figure 2. Synthesis of **P1**. A) Solid phase peptide synthesis (SPPS) by Fmoc strategy consists in cycles of deprotection and amide coupling reactions to yield the linear peptide sequence. B) The final amino group of the peptide is terminated by acylation. C) Mtt selective removal allows the "*on resin*" incorporation of the Boc protected hydrazides pendants. D) TFA treatment cleaves the peptide from the solid support and removes all lateral protective groups to afford **P1**.

selective cleavage, under slightly acidic conditions, of the methyltrityl (Mtt) group (Fig. 2 in red) allowed the "*on resin*" amide coupling of the hydrazide connector **2** that was synthesized in a single step from glutaric anhydride and tert-butylcarbazate (Fig. 2 and ESI). The resin was finally treated with strong acid (TFA) for the deprotection of the side chain protecting groups and cleaved from the solid support (Fig. 2). The peptide was precipitated in Et_2O, centrifuged and thoroughly washed with Et_2O. The solid residue was re-dissolved in water, purified by reverse phase HPLC and characterized (see ESI and Fig. S1). The peptide sequence was designed to give rise to an amphiphilic alpha helix where the two reactive hydrazides would be aligned and at the interphase between the cationic and the hydrophobic domains (Fig. 1). The peptide (**P1**) showed a low helical content in PBS buffer but helicity increased after conjugation with certain aldehydes (*vide infra*). Treatment of peptide **P1** with different aldehydes afforded the corresponding hydrazones after two-hour incubation in DMSO/H_2O (1:1) at 60 °C (Fig. 3 and Fig. S2, see ESI for details). These physiological compatible conditions allowed the direct combination of the hydrazone-modulated peptides with a DNA plasmid and the screening of the corresponding polyplexes for gene delivery.

Polyplex screening. We started transfection experiments in HeLa cells with a plasmid that encoded for the expression of the enhanced green fluorescent protein (EGFP). For transfection experiments, after hydrazone formation, the amphiphilic peptides were readily incubated with the plasmid DNA (pEGFP-C1) in standard Dulbecco's Modified Eagle's Medium (DMEM) for 30 min at room temperature (see ESI). The polyplexes were diluted in DMEM and incubated with HeLa cells for 4 hours. The medium was then replaced and the fluorescence was quantified using a plate reader at 72 hours post-transfection (Fig. 4, Fig. 5A and 5B, see ESI for details). The fluorescence intensity in arbitrary units was

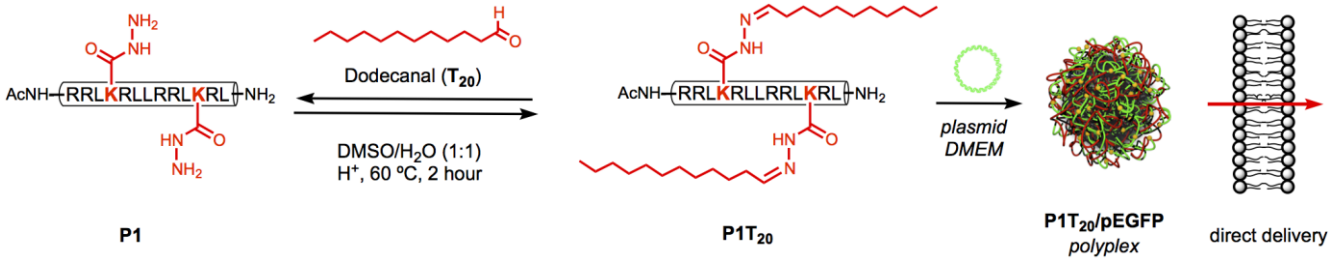

Figure 3. In hydrazone-modulated peptides (e.g. **P1T$_{20}$**), a parent peptide (e.g. **P1**) and aldehyde tails (e.g. dodecanal **T$_{20}$**) are connected *via* a hydrazone linkage. The physiological compatible conditions allowed the direct combination, without any purification or isolation steps, with a plasmid DNA in standard cell culture medium (e.g. DMEM) and the subsequent screening for polyplex delivery in HeLa cells (see Figure 4).

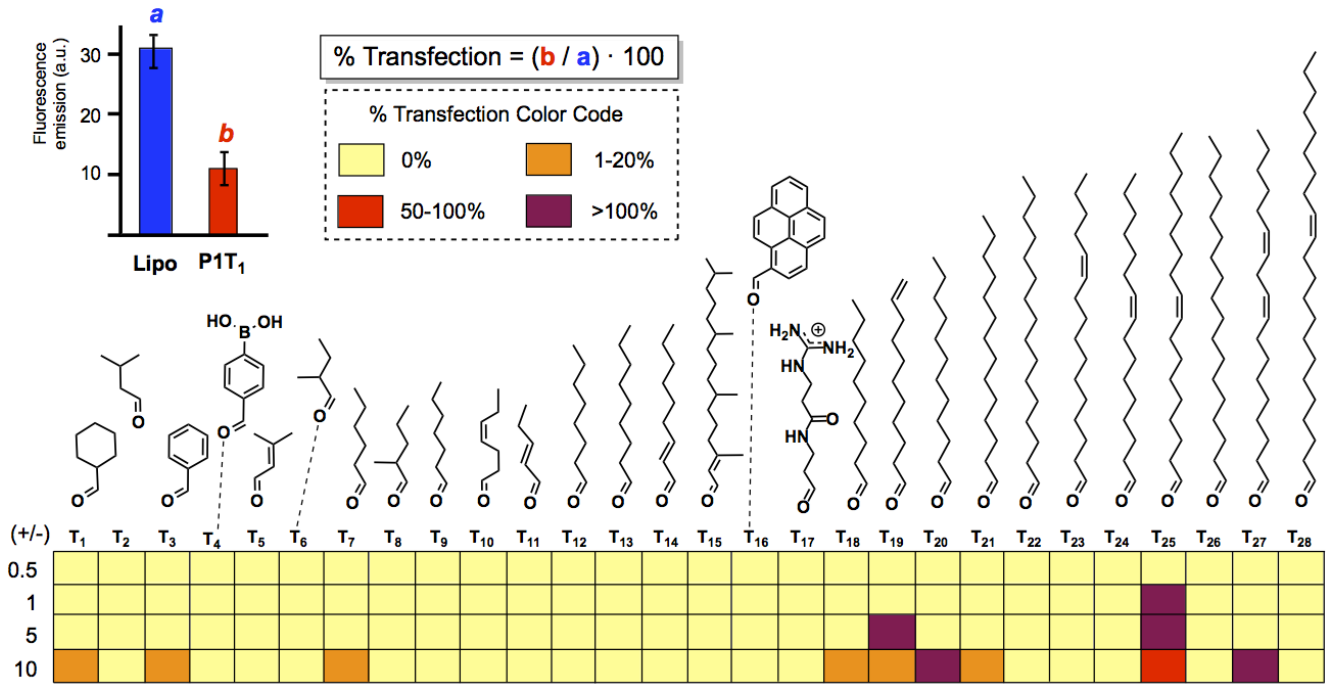

Figure 4. Heat map for the preliminary screening of **P1** with the different aldehyde tails at different charge (+/-) ratios (10, 5, 1, 0.5). All data were obtained from the transfection experiments in HeLa cells and normalized to the 100 % transfection that was assigned to the corresponding control experiments with the commercial reagent Lipofectamine 2000. All data were obtained from triplicate transfection experiments.

normalized against a control experiment with Lipofectamine 2000 (Fig. 4). To perform a broad screening of tails we initially performed transfection experiments at four fixed charge (+/-) ratios for a selection of 28 different aldehydes tails (Fig. 4).

We could confirm that short aliphatic and aromatic aldehydes did not perform as good activators for the transport of plasmid DNAs, although a slight level of transfection was observed for cyclohexanecarboxaldehyde (**T_1**), benzaldehyde (**T_3**) and hexanal (**T_7**) (Fig. 4). However, as previously observed for the delivery of siRNA with peptide dendrons,[28] the best aldehyde activators were long unsaturated hydrophobic molecules (Fig. 4). From this first screening we could identify 10-undecenal (**T_{19}**), dodecanal (**T_{20}**), oleic aldehyde (**T_{25}**) and linoleic aldehyde (**T_{27}**) as the best hydrophobic tails to activate plasmid delivery (Fig. 4). Dodecanal (**T_{20}**) was the only fully aliphatic molecule that triggered plasmid delivery with an efficiency comparable to the commercial reagent Lipofectamine 2000 (Fig. 4). Remarkably, the unsaturated oleic aldehyde was able to efficiently deliver the plasmid DNA at three different charge (+/-) ratios (1, 5 and 10). We therefore decided to fix the best charge ratio of the four best hits (**$P1T_{19}$**, **$P1T_{20}$**, **$P1T_{25}$** and **$P1T_{27}$**) and perform dose-response transfection experiments (Fig. 5C). These experiments confirmed the unsaturated linoleic and oleic aldehydes as the best tails for plasmid transfection, leading to even higher transfection efficiencies than Lipofectamine 2000 (Fig. 5B). Interestingly, although dodecanal (**T_{20}**) did not achieve the best efficiency, this aldehyde tail maintained a good transfection activity even at the lowest concentration of 1 μM (Fig. 5C).

We next evaluated the toxicity of the hydrazone-modulated peptides (Fig. 5D). We employed the colorimetric MTT assay that quantifies cell viability by measuring the mitochondrial activity upon reduction of Thiazolyl Blue Tetrazolium Blue (MTT) to the purple formazan (see ESI for details). We could confirm that, at the working concentrations of the transfection experiments for three of the hydrazone-modulated peptides (i.e. **$P1T_{20}$**, **$P1T_{25}$** and **$P1T_{27}$** at 10 and 5 μM), the cell viability was higher than that observed for the Lipofectamine 2000 transfection experiments (Fig. 5D). The 10-undecenal (**T_{19}**), with an odd number of carbon atoms, showed some toxicity at the higher concentrations (Fig. 5D).

Flow cytometry analysis was performed in order to validate and further quantify the transfection efficiency of hydrazone-modulated peptides (Fig. S3). **$P1T_{25}$** (5 μM) was combined with the plasmid pEGFP-C1 at a charge ratio (+/-) of 5 (see ESI for details). The resulting polyplex exhibited a 70% of GFP positive cells from the total cell counts (Fig. S3). This 70% was comparable with the control experiment carried out with Lipofectamine 2000 (Fig. S3D). However, although the percentage of transfected cells was similar for **$P1T_{25}$** and Lipofectamine 2000, the total number of cells was more than ten times higher for the peptide vector (Fig. S3D).

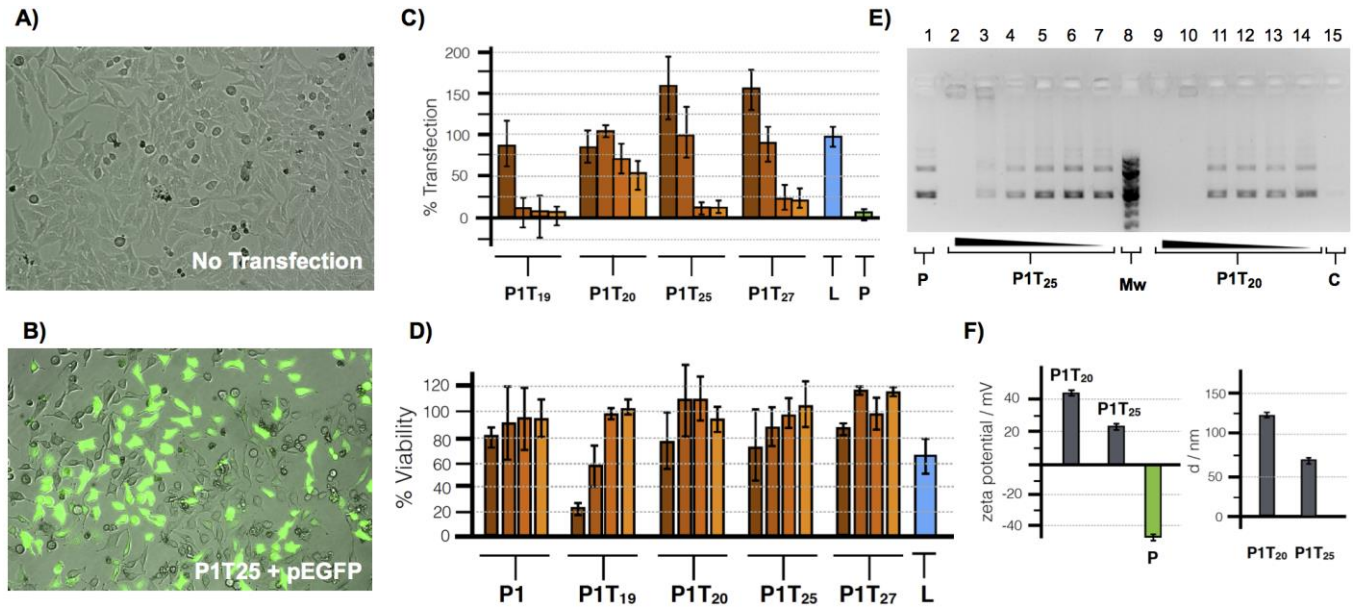

Figure 5. HeLa cells transfection and polyplex characterization. A) and B) Superimposed differential interference contrast (DIC) and epifluorescence image in the green channel. A) Control of HeLa cells with plasmid alone. B) After transfection with **P1T$_{25}$** + pEGFP-C1 C) Normalized transfection efficiency at 4 different concentrations (10, 5, 2.5 and 1 µM from left to right) of peptide **P1** conjugated with the tails: **T$_{19}$** (10-undecenal), **T$_{20}$** (dodecanal), **T$_{25}$** (oleic aldehyde) and **T$_{27}$** (linoleic aldehyde) at a fixed charge ratio of 5 for **P1T$_{19}$** and **P1T$_{25}$** and a fixed charge ratio of 10 for **P1T$_{20}$** and **P1T$_{27}$**. In blue the results with Lipofectamine 2000 and in green the control with the plasmid alone. D) Cell viability obtained by the MTT assay of the different peptides (**P1T$_n$**) at 4 different concentrations (10, 5, 2.5 and 1 µM from left to right) and Lipofectamine 2000. E) Gel retardation assay. *Lane 1*: plasmid alone; *Lanes 2-7*: **P1T$_{25}$** at 6 different charge ratios (10-0.01); *Lane 8*: Molecular weight marker; Lanes 9-14: **P1T$_{20}$** at 6 different charge ratios (10-0.01); *Lane 15*: empty control experiment. [eGFP plasmid DNA] = 0.5 ng/µL in all cases. F) Dynamic light scattering and zeta potential of the plasmid alone and the corresponding DNA/peptide complexes at a 10 charge (+/-) ratio. Values in C) D) F) represent the average of three replicates with the corresponding standard deviation.

To study and characterize the polyplexes upon packing of the plasmid DNA, we carried out a gel retardation assay and we measured dynamic light scattering (DLS) and zeta potential of the peptide conjugated to the oleic aldehyde (**P1T$_{25}$**) and the dodecanal (**P1T$_{20}$**). Not surprisingly, gel electrophoresis confirmed DNA condensation at the corresponding charge (+/-) ratio and peptide concentration that were employed in transfection experiments (Fig. 5E). Dynamic light scattering (DLS) measurements after incubation of hydrazone-modulated peptides with the plasmid DNA revealed polyplexes of 122 nm for the dodecanal (**P1T$_{20}$**) and about 65 nm for the oleic aldehyde (**P1T$_{25}$**) (Fig. 5F and Figs. S4, S5). Size and globular shape of peptide polyplexes were confirmed by atomic force microscopy (AFM) and transmission electron microscopy (TEM) (Figs. S6 and S7, see ESI for details). The zeta (ζ) potential confirmed a positive charged surface for both polyplexes of 45 mVs for **P1T$_{20}$** and of 23 mVs for **P1T$_{25}$** (Fig. 5F). To study the stability of the polyplexes we measured a time course DLS of the peptide/DNA conjugates (Fig. S5). These experiments showed a progressive time dependent increase in the size and in the polydispersity index (PDI) of the polyplexes. This observation suggested a progressive particle aggregation and decomposition of the conjugates between DNA and the hydrazone-modulated peptide with oleic aldehyde and dodecanal tails (Fig. S5). In clear contrast, when the parent peptide without any hydrophobic tail was combined with the plasmid DNA, the PDI was already high at time zero (Fig. S5). The strong polydispersity for **P1** without aldehyde tails clearly confirmed the

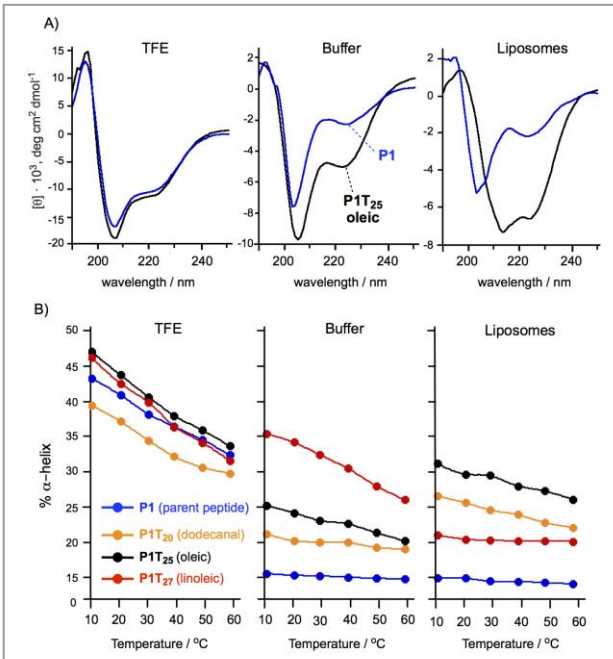

Figure 6. A) CD spectra of **P1** (blue) and **P1T$_{25}$** (oleic aldehyde, black) in TFE, aqueous buffer (HKR, pH = 7.4) and liposomes. B) % of α-helix *vs* the temperature for **P1** (blue), **P1T$_{27}$** (red), **P1T$_{25}$** (black) and **P1T$_{20}$** (orange).

importance of hydrophobic tails to obtain stable and functional nanoparticles.

Circular Dichroism. In order to gain further experimental details into the amphiphile structural properties and helical character, circular dichroism (CD) was measured for three hits (**P1T$_{20}$**, **P1T$_{25}$** and **P1T$_{27}$**) and the parent peptide (**P1**), in three different conditions: trifluoroethanol (TFE), aqueous buffer (pH = 7.4) and liposomes (Fig. 6 and Fig. S8, see ESI for details). We could observe that hydrazone conjugation with the hydrophobic tails increased the helical content of the parent peptide in aqueous conditions and in liposomes (Fig. 6A). This increase in the helicity of the peptide was not observed in the presence of trifluoroethanol, a less competitive solvent for intramolecular hydrogen bonding. The maximum percentage of helicity in aqueous conditions (around 35%) was achieved for **P1** after hydrazone formation with the long unsaturated linoleic aldehyde tail (**T$_{27}$**) (Fig. 6). However, this strong helicity of **P1T$_{27}$** was sensitive to temperature increase of the buffered solutions (Fig. 6B in buffer). In contrast, the highest helical content in liposomes was achieved for the **P1T$_{25}$**, the hydrazone peptide containing the oleic aldehyde (Fig. 6B in liposomes). Intriguingly, the helicity was very stable even at higher temperatures when the peptides where incorporated into the lipid bilayer (Fig. 6B). The peptide with the dodecanal tail (**P1T$_{20}$**) showed an intermediate level of helical increase in buffer and in liposomes (Fig. 6). Taken together, these observations revealed the impact of the aldehyde tails in the secondary structure of the peptide, a condition that was probably due to the enhanced hydrophobic effect in water and to the potential interactions with the hydrophobic part of the lipid bilayer (Fig. 6A).

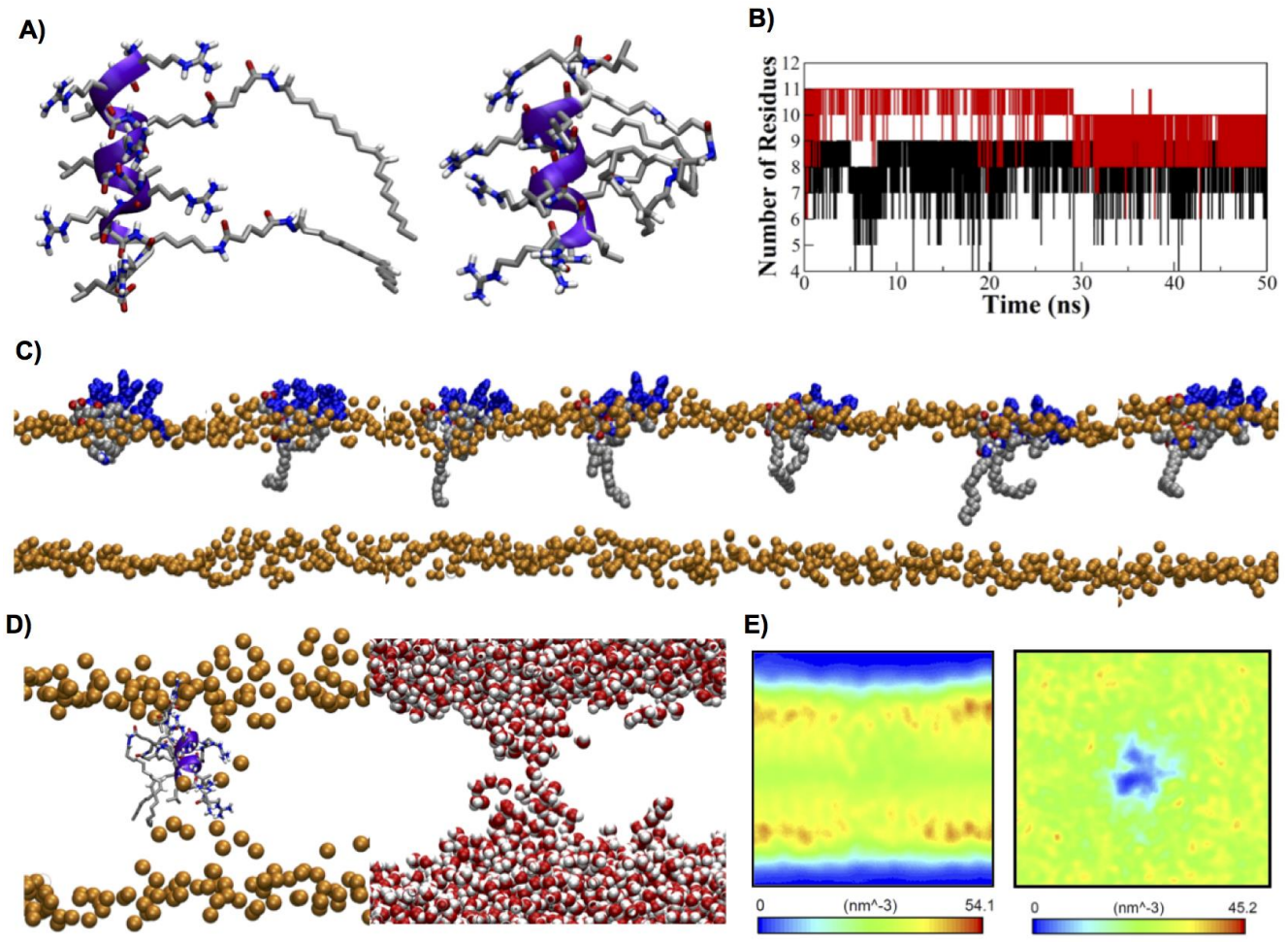

Figure 7. Computational Chemistry. A) Structures of **P1T$_{25}$** at *t* = 0 and *t* = 30 ns from its simulation in H_2O. B) Secondary structure evolution (number of residues in helix + turn) along the MD trajectory for **P1** precursor (black) and **P1T$_{25}$** (red). C) Different snapshots at *t* = 0, 5, 10, 20, 30, 40 and 50 ns from the simulation of **P1T$_{25}$** approaching the surface of a POPC bilayer, applying an electric potential of 0.01 V/nm. A vdW representation is used for the peptide, where the Arg residues are in blue and the peptide backbone and the hydrophobic tails (**T$_{25}$**) in grey. D) Snapshot at *t* = 50 ns from the simulation of **P1T$_{25}$** inserted in a POPC membrane. Only the peptide (in grey) and the lipids phosphorous atoms (in ochre) are represented for clarity. Water molecules in the analogous picture show the *wetting* of the hydrophobic core of the membrane. E) Density maps of lipids along the MD simulations of **P1T$_{25}$** inserted into a POPC bilayer, averaged for 50 ns.

Computational Chemistry

In order to get further insights in the peptide structural behaviour and mode of action, we performed series of all-atoms Molecular Dynamics (MD) simulations of the parent peptide **P1** precursor and **P1T$_{25}$** (Fig. 7 and ESI). We started from a preformed alpha helix and we studied the stability of this helix in water and in membranes. When inserted into a 1-palmitoyl-2-oleoyl-sn-glycero-3-phosphocholine (POPC) lipid bilayer, the peptide bearing the hydrazone hydrophobic tails showed a slightly higher stability compared with the parent peptide **P1** (Fig. 7B). This observation matches with the enhanced helicity, experimentally observed by circular dichroism, for **P1T$_{25}$** in liposomes (Fig. 6A). Interestingly, we could observe that, during the MD simulation in water, the oleic tails of **P1T$_{25}$** embrace the peptide backbone to minimize water repulsion (Fig. 7A). If this "*hugged*" peptide is approached to a POPC membrane, the peptide anchors to the membrane by inserting its hydrophobic tails into the bilayer. Interestingly, very shortly after landing on the membrane, the hydrophobic tails quickly untied from the backbone of the peptide to extend themselves into the hydrophobic core of the bilayer (Fig. 7C, Movie S1). This tail folding/unfolding process suggested that the hydrophobic side chains allowed the dynamic peptide reorganization in response to different environments (Fig. 7C). MD simulations of a membrane pre-inserted amphiphilic peptide (**P1T$_{25}$**) showed an important disruption of the lipidic structure (Fig. 7D and 7E). The peptide was not comfortable into the membrane and water was introduced into the bilayer hydrophobic core (Fig. 7D). This "*wetting*" of the inner leaflet lead to the production of invaginations and to strong lipid reorganization, an observation that could be related with the formation of membrane transient pores from where the cargo might be released (Fig. 7E).[26,42-44] The density maps of the lipids in Fig. 7E suggested a strong disorganization of the bilayer around **P1T$_{25}$**. This membrane reorganization is a consequence of the severe tilting, with respect to the membrane plane, of the lipids that surround the peptide (Fig. S9).

Discussion

The objective of this work was to demonstrate that hydrazone conjugation enables to modulate the activity of a parent linear penetrating peptide in the delivery of a plasmid DNA. The results reported here confirmed a straightforward methodology involving the preparation and rapid screening of amphiphilic pseudo-helical peptides for gene transfection (Figs. 1-4). This approach confirmed several combinations (**P1T$_{19}$**, **P1T$_{20}$**, **P1T$_{25}$** and **P1T$_{27}$**) that performed as non-toxic and efficient plasmid delivery vehicles (Fig. 5). Some of these combinations (i.e. **P1T$_{25}$**) worked with better efficiency and lower toxicity than the commercial reagents usually employed in plasmid transfection experiments of biochemistry and cell biology laboratories (i.e. Lipofectamine 2000) (Fig. 5). As it should be expected, two of the best hits obtained (**P1T$_{20}$** and **P1T$_{25}$**) efficiently packed the plasmid DNA at the optimal charge (+/-) ratio (Fig. 5E). Dynamic light scattering of these two hits confirmed the formation of nanoparticles with a positive zeta potential (Fig. 5F). The protocol was simple and allowed the straightforward identification of three peptides that performed as optimal formulations for plasmid delivery. The hydrazone modulation was carried out in physiological compatible conditions. Therefore, the final amphiphilic peptides were readily combined with the DNA and incubated with the cells, without the need of any isolation or purification steps and/or any other special treatment (i.e. Opti-MEM). Circular dichroism in water and in liposomes indicated an increase in the helical character of the peptides after the conjugation with the hydrophobic tails (Fig. 6). This increase was particularly important for the most efficient amphiphilic peptides bearing long unsaturated hydrophobic tails such as oleic (**T$_{25}$**) and linoleic (**T$_{27}$**) aldehydes. Computational chemistry revealed that the hydrophobic tails flipped over the peptide backbone in aqueous buffer. However, these tails were extended again to anchor the peptide to the membrane and to span the lipid bilayer. This observation suggests that the flexibility of the hydrophobic tails may play an important role in the anchoring process of the peptide to the lipid membrane. In the reported ensemble peptide folding and polyplex formation are controlled by thermodynamics and kinetics.[45] As shown by DLS, the hydrophobic tails were crucial for polyplex formation and stability (Figs. S4 and S5). Enthalpy driven hydrogen bonds would be responsible for peptide helicity but the entropic contribution of the hydrophobic tails seems to be of great importance for the formation of functional polyplexes. However, we should always consider the importance of counterion exchange.[46] This counterion complexes are thermodynamically very stable but kinetically very labile.[46] The importance of the hydrophobic counterion exchange of polyarginines, such as with oleic acid, has experimentally and computationally been described as critical for the translocation of cell penetrating peptides across the lipid bilayer.[46-48] Although more experiments would be needed to confirm this hypothesis, this hydrophobic folding/unfolding behaviour could have important implications in both the DNA packing and the cargo delivery of hydrazone-modulated peptides. As previously described for other non-viral gene delivery systems, the recombination of charges (+/-) during the delivery process could lead to the formation of pores, or membrane holes, from where the cargo can escape and perform its corresponding function.[26,42-44] Interesting implications of the phase transition from lamellar to hexagonal[43] and gyroid cubic phases[13] have been studied for lipoplexes.[13,43] Recently, it has been proposed that the monomer release from the supramolecular nanoparticles is the critical step to achieve an efficient delivery and not the particular nanoparticles themselves (poly or lipoplexes).[26] Nevertheless, the presence of hydrophobic flexible pendants seems to be a critical structural feature for penetrating peptides in order to trigger the efficient delivery of supramolecular conjugated payloads such as nucleotides and proteins.[23,24]

The purpose of this paper was to validate the methodology of hydrazone modulation for nucleotide transport across the cell membrane. We have applied this methodology for the particular case of linear peptides and plasmid transfection, two key features that were not demonstrated before.[27,28,37,40,41] We hypothesize that changes in peptide topology modulate peptide shape and transient amphiphilicity and thus might affect critical steps in the delivery process such as the interaction with nucleotides and anionic

membrane components,[19] the disruption of the membrane integrity and the escape of the cargo.[26-28] We believe that we should pay attention to the molecular level features of non-viral vectors in order to understand and improve the efficacy of the bigger nanoplexes.[13,26] In this study we have strictly focused in the hydrazone modulation from the synthetic and screening point of view. However, we hope that at due time, not only the synthetic, but also the dynamic properties of the hydrazone bond will help us in understanding and developing novel and improved gene and drug delivery vehicles.

Conclusions

Independently of the nature of the different nucleotides required for gene therapy they all need to be efficiently delivered. Therefore, the development of new tools for nucleotide delivery stands as a major challenge for chemistry and materials science. In this paper we have developed the hydrazone modulation of a parent penetrating peptide to trigger the cellular transfection of a DNA plasmid. This approach allowed us to identify three hydrazone modulated amphiphilic peptides that delivered a plasmid DNA in HeLa cells with better efficiency and less toxicity than the standard commercial reagents employed in routine transfection experiments.

Experimental Methods

Detailed methods and protocols for peptide synthesis and characterization, cell transfection and viability experiments, microscopy images as well as computational methods can be found in the electronic supplementary information (ESI) online.

Acknowledgements

We are thankful to Dr. Irene Lostalé-Seijo for cell culture assistance and discussions. We acknowledge funding from the Spanish Government MINECO: [CTQ2014-59646-R] and [CTQ2015-74621-JIN], the Xunta de Galicia (ED431G/09), the ERDF and the CESGA. R. G.-F. received a FCT Investigator Grant from Portugal (IF/01133/2015). J.M. received a Ramon y Cajal (RYC-2013-13784) and an ERC Starting Investigator Grant (DYNAP-677786).

Notes and references

1 A. B. Hill, M. Chen, C.-K. Chen, B. A. Pfeifer and C. H. Jones, *Trends Biotechnol.*, 2016, **34**, 91–105.
2 D. B. T. Cox, R. J. Platt and F. Zhang, *Nat. Med.*, 2015, **21**, 121–131.
3 H. Yin, R. L. Kanasty, A. A. Eltoukhy, A. J. Vegas, J. R. Dorkin and D. G. Anderson, *Nat. Rev. Genet.*, 2014, **15**, 541–555.
4 C. Sheridan, *Nat. Biotechnol.*, 2011, **29**, 121–128.
5 M. A. Kay, *Nat. Rev. Genet.*, 2011, **12**, 316–328.
6 R. Kanasty, J. R. Dorkin, A. Vegas and D. Anderson, *Nat. Mater.*, 2013, **12**, 967–977.
7 Z. Li and T. M. Rana, *Nat. Rev. Drug. Discov.*, 2014, **13**, 622–638.
8 U. Sahin, K. Karikó and Ö. Türeci, *Nat. Rev. Drug. Discov.*, 2014, **13**, 759–780.
9 W. B. Kauffman, T. Fuselier, J. He and W. C. Wimley, *Trends Biochem. Sci.*, 2015, **40**, 749–764.
10 Y. Zhang, A. Satterlee and L. Huang, *Mol. Ther.*, 2012, **20**, 1298–1304.
11 G. Gasparini, E.-K. Bang, J. Montenegro and S. Matile, *Chem. Commun.*, 2015, **51**, 10389–10402.
12 A. G. Kohli, P. H. Kierstead, V. J. Venditto, C. L. Walsh and F. C. Szoka, *J. Control. Release*, 2014, **190**, 274–287.
13 C. R. Safinya, K. K. Ewert, R. N. Majzoub and C. Leal, *New. J. Chem.*, 2014, **38**, 5164–5172.
14 P. Yingyuad, M. Mével, C. Prata, S. Furegati, C. Kontogiorgis, M. Thanou and A. D. Miller, *Bioconjugate Chem.*, 2013, **24**, 343–362.
15 F. Cardarelli, L. Digiacomo, C. Marchini, A. Amici, F. Salomone, G. Fiume, A. Rossetta, E. Gratton, D. Pozzi and G. Caracciolo, *Sci. Rep.*, 2016, **6**, 25789.
16 T. Lehto, K. Ezzat, M. J. A. Wood and S. E. Andaloussi, *Adv. Drug. Deliv. Rev.*, 2016, **106**, 172–182.
17 T. Kato, H. Yamashita, T. Misawa, K. Nishida, M. Kurihara, M. Tanaka, Y. Demizu and M. Oba, *Bioorg. Med. Chem.*, 2016, **24**, 2681–2687.
18 P. Boisguerin, S. Deshayes, M. J. Gait, L. O'Donovan, C. Godfrey, C. A. Betts, M. J. A. Wood and B. Lebleu, *Adv. Drug. Deliv. Rev.*, 2015, **87**, 52–67.
19 I. Nakase, H. Akita, K. Kogure, A. Gräslund, Ü. Langel, H. Harashima and S. Futaki, *Acc. Chem. Res.*, 2012, **45**, 1132–1139.
20 J. Hoyer and I. Neundorf, *Acc. Chem. Res.*, 2012, **45**, 1048–1056.
21 H. Tang, L. Yin, K. H. Kim and J. Cheng, *Chem. Sci.*, 2013, **4**, 3839–3844.
22 D. Abegg, G. Gasparini, D. G. Hoch, A. Shuster, E. Bartolami, S. Matile and A. Adibekian, *J. Am. Chem. Soc.*, 2017, **139**, 231–238.
23 Z. Meng, L. Luan, Z. Kang, S. Feng, Q. Meng and K. Liu, *J. Mat. Chem. B*, 2017, **5**, 74–84.
24 S. Futaki, W. Ohashi, T. Suzuki, M. Niwa, S. Tanaka, K. Ueda, H. Harashima and Y. Sugiura, *Bioconjugate Chem.*, 2001, **12**, 1005–1011.
25 K. Kostarelos and A. Miller, *Chem. Soc. Rev.*, 2005, **34**, 970–994.
26 S. Vaidyanathan, B. G. Orr and M. M. Banaszak Holl, *Acc. Chem. Res.*, 2016, **49**, 1486–1493.
27 J. M. Priegue, D. N. Crisan, J. Martínez-Costas, J. R. Granja, F. Fernandez-Trillo and J. Montenegro, *Angew. Chem. Int. Ed.*, 2016, **55**, 7492–7495.
28 C. Gehin, J. Montenegro, E.-K. Bang, A. Cajaraville, S. Takayama, H. Hirose, S. Futaki, S. Matile and H. Riezman, *J. Am. Chem. Soc.*, 2013, **135**, 9295–9298.
29 M. E. Davis, J. E. Zuckerman, C. H. J. Choi, D. Seligson, A. Tolcher, C. A. Alabi, Y. Yen, J. D. Heidel and A. Ribas, *Nature*, 2010, **464**, 1067–1070.
30 J. Liu, W. E. Hennink, M. J. van Steenbergen, R. Zhuo and X. Jiang, *Bioconjugate Chem.*, 2016, **27**, 1143–1152.
31 E. Bartolami, C. Bouillon, P. Dumy and S. X. B. Ulrich, *Chem. Commun.*, 2016, **52**, 4257–4273.
32 V. Bagnacani, V. Franceschi, M. Bassi, M. Lomazzi, G. Donofrio, F. Sansone, A. Casnati and R. Ungaro, *Nat. Commun.*, 2013, **4**, 1721.
33 E. Bartolami, Y. Bessin, V. Gervais, P. Dumy and S. Ulrich,

Angew. Chem. Int. Ed., 2015, **54**, 10183–10187.
34 G. Gasparini, G. Sargsyan, E.-K. Bang, N. Sakai and S. Matile, *Angew. Chem.*, 2015, **54**, 7328–7331.
35 G. Gasparini, E.-K. Bang, G. Molinard, D. V. Tulumello, S. Ward, S. O. Kelley, A. Roux, N. Sakai and S. Matile, *J. Am. Chem. Soc.*, 2014, **136**, 6069–6074.
36 A. van den Berg and S. F. Dowdy, *Curr. Opin. Biotech.*, 2011, **22**, 888–893.
37 J. Montenegro, E.-K. Bang, N. Sakai and S. Matile, *Chem. Eur. J.*, 2012, **18**, 10436–10443.
38 J. Montenegro, A. Fin and S. Matile, *Org. Biomol. Chem.*, 2011, **9**, 2641–2647.
39 J. Montenegro, J. Braun, O. Fischer-Onaca, W. Meier and S. Matile, *Org. Biomol. Chem.*, 2011, **9**, 6623–6628.
40 J. Montenegro and S. Matile, *Chem. Asian J.*, 2011, **6**, 681–689.
41 J. M. Priegue, J. Montenegro and J. R. Granja, *Small*, 2014, **10**, 3613–3618.
42 I. Hafez, N. Maurer and P. Cullis, *Gene Ther.*, 2001, **8**, 1188–1196.
43 I. Koltover, T. Salditt, J. O. Rädler and C. R. Safinya, *Science*, 1998, **281**, 78–81.
44 Y. Xu and F. Szoka, *Biochemistry*, 1996, **35**, 5616–5623.
45 J. Wang, K. Liu, R. Xing and X. Yan, *Chem. Soc. Rev.*, 2016, **45**, 5589–5604.
46 N. Sakai and S. Matile, *J. Am. Chem. Soc.*, 2003, **125**, 14348–14356.
47 N. Chuard, K. Fujisawa, P. Morelli, J. Saarbach, N. Winssinger, P. Metrangolo, G. Resnati, N. Sakai and S. Matile, *J. Am. Chem. Soc.*, 2016, **138**, 11264–11271.
48 H. D. Herce, A. E. Garcia and M. C. Cardoso, *J. Am. Chem. Soc.*, 2014, **136**, 17459–17467.

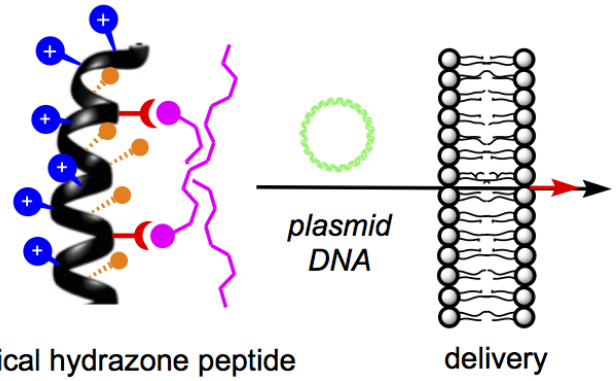

The synthetic potential of dynamic bond formation is introduced for the delivery of plasmid DNA by modulated amphiphilic peptides. The synthetic advantage of these dynamic bonds allowed the identification of improved reagents (better efficiency and lower toxicity) for plasmid transfection assays in human HeLa cells.